Characteristic Scales of Two-Dimensional Turbulence in Polymer Solutions

Ruri Hidema
Organization of Advanced Science and Technology, Kobe University, Kobe, Hyogo 657-8501, Japan

Hiroshi Suzuki, Shion Hisamatsu, and Yoshiyuki Komoda
Dept. of Chemical Science and Engineering, Kobe University, Kobe, Hyogo 657-8501, Japan

DOI 10.1002/aic.14364
Published online January 24, 2014 in Wiley Online Library (wileyonlinelibrary.com)

An experimental study has been performed to investigate the relationship between the extensional viscosity of polymers and the turbulent drag reduction. Self-standing flowing soap film was used to generate two-dimensional (2-D) turbulent flow to eliminate shear stress. Two types of polymers having different flexibilities were added to the 2-D turbulence. The effects of these polymers were visualized by the interference pattern of flowing soap films. The vortex deformation by adding polymers was analyzed by Fourier transformation and wavelet transformation. The scaling exponents of the power spectrum of interference patterns indicate that the mechanism of turbulence laminarization due to the extensional viscosity is anisotropic. A wavelet analysis reveals the high and low fluctuations of the polymer-added flow. Results from wavelet analysis indicate disappearing of original vortices, and appearing of new structures in low frequency in 2-D flow. © 2014 American Institute of Chemical Engineers *AIChE J*, 60: 1854–1862, 2014
Keywords: two-dimensional turbulence, drag reduction, extensional viscosity, power spectrum, wavelet analysis

Introduction

The addition of small amounts of high-molecular-weight linear chain polymers in a Newtonian flow causes a large reduction of frictional drag in a pipe flow. This phenomenon was discovered in 1949 and is referred to as the drag reduction effect.[1] A classical technique to quantify the drag reduction effect is to observe the friction factor by measuring the pressure drop along the pipe. Although the drag reduction technique has been used in numerous industries to improve energy efficiency, the mechanism of this effect is not completely understood. This is due to the complex behaviors of polymers in solution and in turbulent flow, that is, polymer molecules are coiled in a spherical shape when at rest, and can be uncoiled and stretched under the stress exerted on them by a fluid.

Lumley first proposed that the increase in apparent viscosity in the flow outside the viscous sublayer due to the molecular extension of polymers may be a key to drag reduction.[2,3] Virk and Wagger[4,5] also suggested that the polymers are only effective when they are elongated, for example, in a rod or an extended thread. Many studies have attempted to examine these hypotheses by using numerical and experimental analysis. Because the polymer extension induces anisotropic effects on turbulence, Toonder et al.[6] described the turbulence affected by viscous anisotropic effects are caused by the polymer extension and orientation. In their research, it was proposed that the polymer additives do not simply suppress the turbulent motion. On the contrary, the streamwise turbulence intensity is for example increased, whereas the normal turbulence intensity is decreased. This meant that the turbulence structure was changed, rather than attenuated. Vast researches have tried to investigate the reason of this anisotropic effect. Smith et al. made a first experimental work that visualized the stretching of DNA molecules by extensional flow.[7] Owing to this work, the polymer extensions in turbulent flow became real. Such an extension of polymers induces extensional viscosity, which is the resistance of the extension in extensional direction, of polymers. Extensional viscosity of polymers can reach much higher values compared to the intrinsic viscosity, which is related to the shear viscosity (Figure 1a). Indeed, the nonzero normal stress differences, which are related to the extensional viscosity, decrease in shear flows and increase, often by several orders of magnitude, in extensional flows.[8] Therefore, recently many researchers consider that an abrupt increase in the extensional viscosity that depends on the extensional strain rate in turbulence is a key in turbulent drag reduction.[9,10] Recent researches of direct numerical simulations of the drag reduction effects also shows the importance of the extensional viscosity, which changes the velocity field of buffer layer between the logarithmic region and the viscous boundary layer.[9,11–15]

On the other hand, effects of the elasticity due to polymers have also been studied. Housiadas and Beris have studied the viscoelastic effects on turbulent drag reduction by numerical simulation.[16–18] They made a pioneering work taking care of relaxation times and fading memory effects of polymers. Effects of the elasticity due to relaxation are also mentioned in some experimental results.[19]

Correspondence concerning this article should be addressed to R. Hidema at hidema@port.kobe-u.ac.jp.

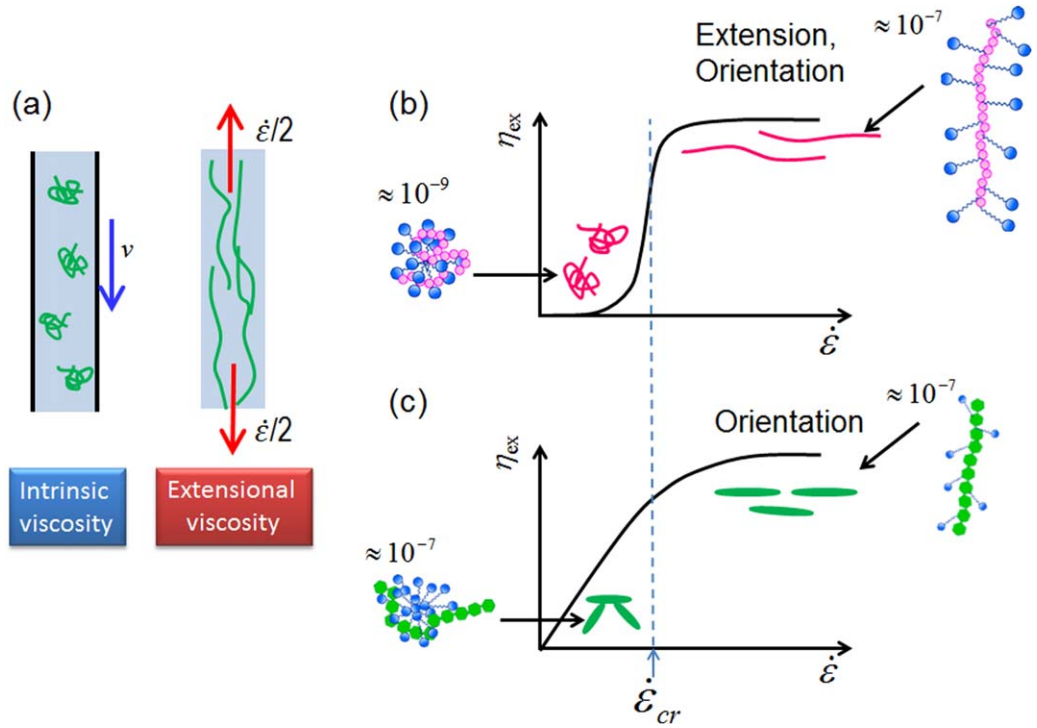

Figure 1. Schematic of the extensional viscosity.

(a) The extension of polymers generates extensional viscosity. (b) Flexible and (c) rod-like rigid polymers exhibit different increments of extensional viscosity. [Color figure can be viewed in the online issue, which is available at wileyonlinelibrary.com.]

All these previous studies indicate that drag reduction effects enhance the anisotropic structure, that is, coherent structure in turbulence. When drag reduction occurs, vortices of the turbulence created at a wall become long in streamwise direction.[8,9,20] This variation of the vortices in turbulence changes the energy transfer in turbulence. The energy of the normal velocity component is dramatically suppressed over all frequencies, whereas there is a redistribution of energy from high frequencies to low frequencies in the streamwise component.[6,21,22] Such a variation of the energy transfer leads laminarization of the turbulent flow that is drag reduction effects.

When we again focus on the drag reduction effects due to extensional viscosity, because most of all the previous studies were made in three-dimensional (3-D) flow, it was difficult to eliminate effects of shear stress and to extract the extensional stress completely. Therefore, we focus on 2-D flow to observe the effects of polymers directly affected by extensional stress. Two-dimensional flow can be made by flowing soap films.[23,24] The primary experimental research using flowing soap films in laboratories started in the 1980's by Couder[25,26] and Gharib and Derango.[27] The measurements of the present study were performed by self-standing flowing soap films, which closely follows a design by Rutgers et al.,[28] as shown in Figure 2a. As the detailed explanation is written in section "Experimental apparatus and extensional stress added in the apparatus", the importance of this system is that flowing soap film has free surface. Therefore, the flow is not affected by shear stresses from the wall. Using this system, we separate the extensional stress from the shear stress. In addition, when the grid equally spaced cylinders are inserted to the flow, vortices are generated at the grid. Since velocities of the flowing soap film can reach even 2 m/s, the grid can make 2-D grid turbulence. The 2-D grid turbulence is mainly affected by extensional stress that is induced by the grid as written in section "Experimental apparatus and extensional stress added in the apparatus".

Some biggest differences in 2-D from 3-D turbulence are that 2-D turbulence has two cascade, an inverse energy cascade to large scales and an enstrophy cascade to the small scales, as both energy and enstrophy (mean squared vorticity) are conserved.[23,24] Conservations of enstrophy are due to absence of the vortex stretching in 2-D turbulence. This is because the lateral dimensions of soap films are many orders of magnitude larger than their thickness. These two cascade ranges are believed to be separated by an injection scale l_{inj}. For the scales larger than l_{inj}, inverse energy cascade dominates the flow. For the scales smaller than l_{inj}, enstrophy cascade dominates the flow.[23,24] Although the vortex stretching is absent, thicknesses of 2-D grid turbulence and flowing soap films are fluctuating. Such a fluctuation in the thickness of soap film is a passive scalar.[23,24,29] Batchelor predicted the passive scalar scaling in 2-D turbulence that is affected by inverse energy cascade and enstrophy cascade.[30] Amarouchene and Kellay tried to confirm Batchelor's theory by experimental works, they confirmed the following scaling.[29] When the power spectrum of the thickness fluctuations, $<h^2(f)>$, in turbulent soap films shows scaling behavior, $<h^2(f)> \sim f^{\alpha}$, the index α reflects the passive scalar scaling. Thus, α was $-5/3$ when the passive scalar field was affected by both inverse energy and enstrophy cascades and α became -1 when the passive scalar field was affected only by the enstrophy cascade. In their research, they use single-point measurement by using a laser Doppler velocimetry.

On the basis of all the backgrounds described above, Hidema et al. developed an image analysis to detect the passive scalar scaling, thickness fluctuations, affected by

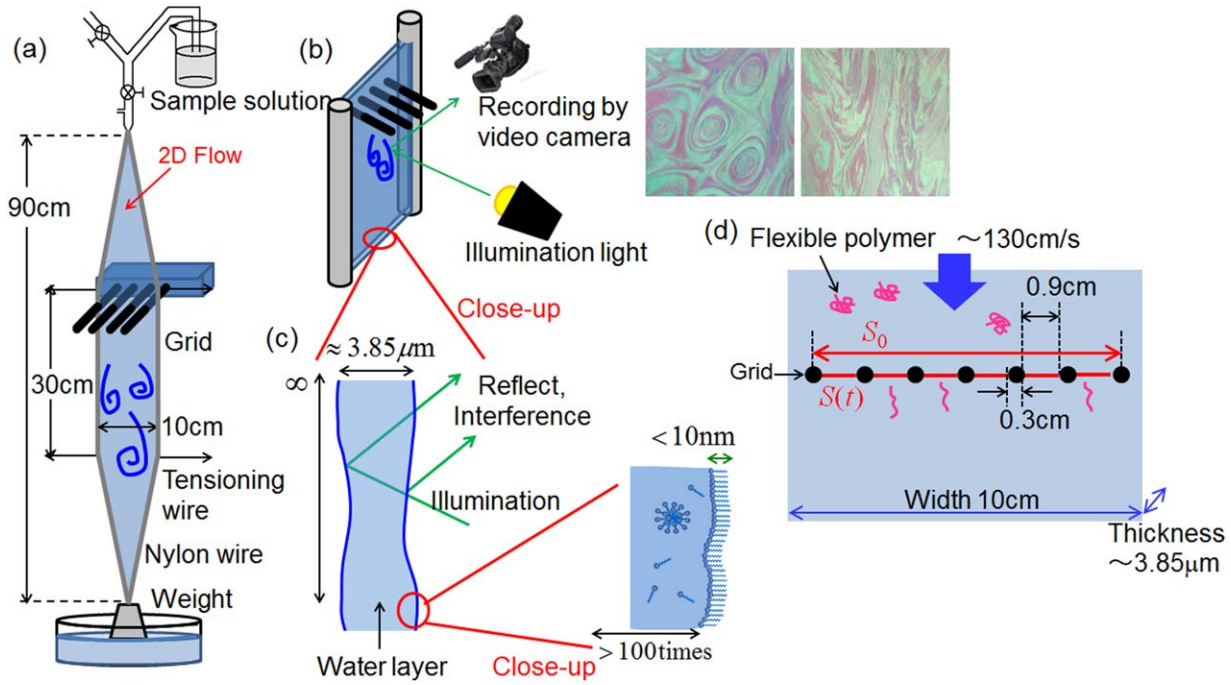

Figure 2. Experimental set-up of flowing soap films.

(a) Whole image, (b) close-up of the flowing soap film channel (2-D flow), and (c) cross-section of a 2-D flow. (d) How the extensional strain occurs in this flow around the grid. [Color figure can be viewed in the online issue, which is available at wileyonlinelibrary.com.]

polymers through interference patterns of flowing soap films.[31] By using this technique, we have studied the effects of polymers in 2-D turbulence. When the polymers affect turbulence, the vortices of 2-D turbulence were deformed. Such a deformation as an output from this system related to the anisotropic structure that can be observed when drag reduction occurs as described above. Therefore, it was important to analyze the deformation of vortices in 2-D flow by image analyses.[10,32,33] In addition, the drag reduction effect differs for flexible and rod-like rigid polymers because flexible polymers stretch abruptly under extensional strain, whereas rod-like rigid polymers gradually become oriented under extensional strain, as indicated by the results for dynamic right scattering and flow birefringence.[10,32] These differences change the effective increase in extensional viscosity (Figures 1b, c). In our previous works, we focused on how extension and orientation of different flexible and rigid polymers add anisotropic effects on deformations of vortices in 2-D flow, which is related to energy transfer.[10,33] From the results, the energy transfers in the normal and streamwise directions were expected to be different. That is, in the normal direction, the orientation of polymers prohibits energy transfer, whereas the extensional viscosity prohibits energy transfer in the streamwise direction due to the stretching of the vortices in the streamwise direction. These results were also obtained from the morphology of the 2-D vortices.

In this study, we report a result of wavelet analyses on 2-D vortices to investigate further the anisotropic effects. The anisotropic effects can be visualized through the vortices deformation, which can be affected by extensional viscosity of flexible and rod-like rigid polymers. A wavelet analysis is an important tool for distinguishing coherent structure from incoherent structure.[23,34–36] Thus, the fluctuation in the streamwise direction was analyzed by wavelet transform. By calculating wavelet coefficients, we can determine the characteristic scale affected by polymers.[23,37–40]

Experimental

Materials

Soap solutions contained sodium dodecylbenzenesulfonate (SDBS) as a surfactant at a concentration of 2 wt%. As flexible polymers, polyethyleneoxide (PEO, molecular weight: 3.5×10^6) was used at concentrations of 0.25, 0.5, 0.75, 1.0, 1.5, and 2.0×10^{-3} wt%. As rod-like rigid polymers, hydroxypropyl cellulose (HPC, molecular weight: $>1.0 \times 10^6$) was used at concentrations of 0.01, 0.03, and 0.05 wt%. The overlap concentration of PEO was approximately 0.012 wt%, and that of HPC was approximately 0.15 wt%.

Experimental apparatus and extensional stress added in the apparatus

The experiments were carried out using the apparatus shown in Figure 2a. This system closely follows a design by Rutgers et al.[28] Two nylon wires were used to make a soap film channel. Soap solutions were flowing under the action of gravity from the top reservoir to the bottom reservoir. Mean velocities reach uniform velocities at about 30 cm behind from the injection nozzle. The mean thickness of the water layer $h(t)$ (m) was 3.85 μm, with a mean velocity $V(t)$ (m/s) of 130 cm/s for a flow flux $Q(t)$ (m^3/s) of 0.5 mL/s. The relationship of $h(t)$, $V(t)$, $Q(t)$, and the width of the soap film channel, W (m), of 10 cm are shown as

$$h(t)=Q(t)/V(t)W \tag{1}$$

When a grid of equally spaced cylinders was inserted to the flow, 2-D turbulent flows appeared (Figure. 2b). As shown in Figure 2c, both sides of the flowing soap films are free surfaces, and the water layer is sandwiched by

surfactants. The surfactant molecule is sufficiently small and the surface area is sufficiently large compared to the thickness of water layer. In addition, the surface tension is negligible due to the surfactant in the surface of flowing soap films. Therefore, soap film is considered to be a 2-D water layer flow.[23,24]

When a grid is inserted into the flow, extensional strain occurs at the grid. When polymers exist in flows, the polymers are affected by the extensional strain which causes polymer stretching or polymer orientation. The extensional strain applied in the apparatus is approximately calculated as follows[33]

$$S(t)=S_0\,exp(-\dot{\varepsilon}t) \tag{2}$$

where S_0 (m^2) is the cross-sectional area of the water layer in flowing soap film before deformation, $S(t)$ (m^2) is the cross-sectional area after deformation. t (s) is the time required for deformation from S_0 (m^2) to $S(t)$ (m^2). In this study, the diameter of the cylinder was 0.3 cm, and the gaps between cylinders were 0.9 cm (Figure 2d). The numbers of cylinders were seven. In the case of Figure 2d, S_0 (m^2) was calculated as 7.20 cm $\times$ 3.85 μm, and 7.20 cm corresponds to the distance between the centers of two end cylinders and 3.85 μm corresponds to the thickness of the water layer. $S(t)$ (m^2) was calculated as 5.40 cm $\times$ 3.85 μm, and 5.40 cm could be calculated by 0.9 cm $\times$ 6, as seven cylinders were used in the case of Figure 2d. t (s) was calculated by the radius of the cylinders and mean velocity of the flow, which is 0.15 cm divided by 130 cm/s. Then, in this case, $\dot{\varepsilon}$ was calculated as about 250 s^{-1}. The extensional rate is considered to lead polymer stretching or polymer orientation.

Turbulence visualization and data acquisition

Soap films reflect illumination light at the front and back surfaces, which generates interference patterns of the film. Because the interference of the illumination lights is affected by the thickness of the water layer, the interference patterns contain information on the dynamics of the water layer as 2-D flows. The film is illuminated by a commercial white light source (EFA25EN/22, TOSHIBA). According to the data sheet provided by the manufacturer, although the wavelengths of this illumination range from 400 to 720 nm, a major narrow peak is at 540 nm. Because the thickness fluctuations in the flowing soap films in a turbulent state are typically only 5%, the thickness fluctuations is calculated as 190 nm in this study.[24,31] Therefore, in this experimental condition, it is considered that the interference patterns mainly results from the wavelength of 540 nm. Thus, variation of interference index can be neglected. Then, it is reasonable to consider the interference pattern is related to the thickness fluctuations of 2-D flows.[30]

The interference images were recorded using a digital video camera (Panasonic TM700) in the data acquisition area, which was located 20 cm behind the grid. The vortices in 2-D flows were generated when solution passes the grid. At that time, polymers in the solution were affected by the extensional stress described by Eq. 2, which induce polymer extension and orientation. Here, relaxation time of polymer should be mentioned. For example, a previous work mentioned relaxation times of PEO, which are less than 10^{-3} s^{-1}.[41] It means that the PEO can be relaxed just after the flow passes the grid. However, the grid turbulence is generated at the grid, and just advected to the downstream. Therefore, even when the PEO is relaxed in a few second, it is possible to observe the vortices affected by PEO in an extensional state. At the position 20 cm behind the grid, Taylor's frozen hypothesis was confirmed.[42] Therefore, the data acquisition area in this study is reasonable. The shutter speed of the video camera was 1/3000 s. The time interval for a series of images was adjusted to 1/60 s. Each of the frames acquired by the camera was converted into an Red-Green-Blue (RGB) file with a spatial resolution of 640 pixels $\times$ 360 pixels. Part of the image that corresponds to the data acquisition area was clipped. The size of the image is 256 pixels $\times$ 256 pixels, which corresponds to 2.56 $\times$ 2.56 cm^2. More precise explanation of this apparatus is written in our previous work.[31]

Image processing by film interference flow imaging

In our previous study, we proposed image analysis to analyze the interference patterns of 2-D flow. This analysis can detect polymer effects on the basis of morphology. Vortices in 2-D flow were analyzed by curvature of the vortices and by 2-D-Fast Fourier Transform (FFT) of the patterns. Two-dimensional flow affected by polymers were reasonably analyzed by the interference patterns, thus, we named this method as Film Interference Flow Imaging (FIFI). In this study, we again use the FIFI method. The interference images were analyzed by 2-D-FFT and a wavelet transformation.

Two-Dimensional-FFT Analysis. Two-dimensional FFT software was used to calculate the power spectrum of the interference images.[31] Because the RGB pixel intensity of the images is related to the thickness of the water layer, the power spectrum of the image reveals the dynamics of 2-D flows. In our experimental condition, especially the pixel intensity G is related to the thickness fluctuation on the basis of wavelength of the illumination light. Therefore, the power spectrum $<I^2(k_x, k_y)>$ was calculated based on the pixel intensity, G, with a Hamming window, where k_x (m^{-1}) and k_y (m^{-1}) are the spatial frequency in the streamwise and normal directions, respectively, in an interference image.[21] For the measurements presented herein, the data acquisition area that was clipped from the video frames was 256 pixels $\times$ 256 pixels, which corresponds to 2.56 $\times$ 2.56 cm^2. Thus, k_x and k_y range from 1/2.56 to 1/0.02 cm^{-1}, that is, 0.391 to 5.00 cm^{-1}, according to the frequency. The power spectrum $<I^2(k_x, k_y)>$ for pixel intensity G characterizes the strength of the thickness fluctuation of the water layer based on spatial frequencies k_x and k_y. Here, the power spectra for both frequencies are plotted to discuss the energy transfer of turbulence in the streamwise and normal directions.

Wavelet Analysis. The wavelet analysis is applied for analyzing the spatial fluctuation of the water layer.[22] Wavelet analysis is a mathematical technique introduced in the 1980's. Contrary to the Fourier transform, the wavelet transform is a mathematical tool that can be used to resolve strongly irregular signals, such as turbulent signals from different scales, while keeping the signals localized both in space and frequency. Wavelet analysis provides a 2-D unfolding of 1-D signals, resolving both the position and the scale as independent variables.[38] Streamwise line data of the pixel intensity G of the image were used for the analysis. The data for approximately 6000 pixels, corresponding to 65 cm, were clipped by connecting approximately 30 consecutive images, where 30 images were captured in 0.5 s, because the time interval in a series of images was 1/60 s.

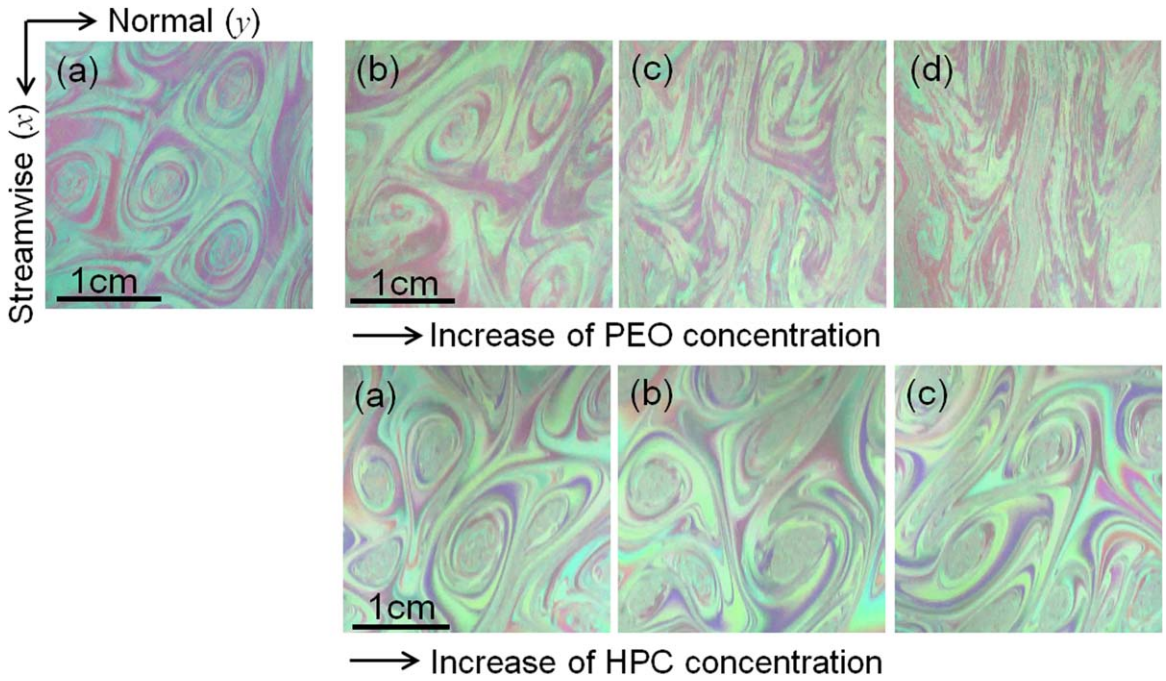

Figure 3. Interference images of the turbulence in flowing soap films.

Images of (a) a SDBS 2 wt% solution, (b) a + PEO 0.5 × 10^{-3} wt% solution, (c) a + PEO 1.0 × 10^{-3} wt% solution, (d) a + PEO 2.0 × 10^{-3} wt%, (e) a + HPC 0.01 wt% solution, (f) a + HPC 0.03 wt% solution, and (g) a + HPC 0.05 wt% solution for a mean velocity of approximately 130 cm/s. The black bar indicates the scale. [Color figure can be viewed in the online issue, which is available at wileyonlinelibrary.com.]

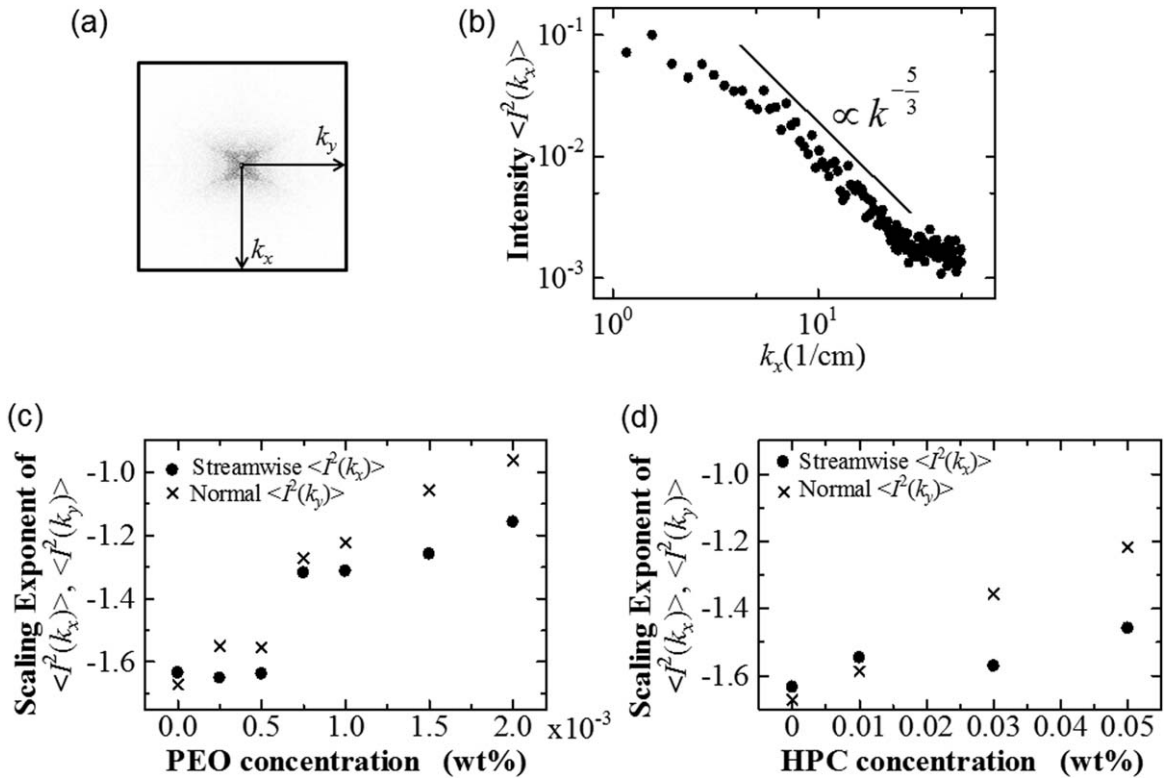

Figure 4. Power spectrum and scaling exponents.

(a) Two-dimensional representation of the power spectrum, $<I^2(k_x, k_y)>$, of the interference image corresponding to Figure 3a. The k_x and k_y directions in the image represent the spatial frequencies in the streamwise and normal directions. (b) Example of the scaling form of the power spectrum. (c) Scaling exponents of the power spectra in each direction for (a) PEO additives. (d) Scaling exponents of the power spectra in each direction for (b) HPC additives.

The wavelet transform coefficient, $W(a, b)$, is defined for a streamwise water layer fluctuation of intensity G, $G(x)$, as follows

$$W(a,b)=\frac{1}{\sqrt{a}}\int \phi\left(\frac{x-b}{a}\right)G(x)dx \tag{3}$$

where x (m) is the length scale, and a (m) and b (m) are wavelet scale and sequence scale parameters, respectively. The function $\phi(X)$ is defined as the mother wavelet, which is localized around $x=0$. The performance of this analysis is determined by the choice of the analyzing wavelet $\phi(X)$. In this study, the mother wavelet $\phi(X)$ on a variable X, the "Mexican hat" wavelet, is adopted as follows

$$\phi(X)=\left(1-X^2\right)e^{-\frac{X^2}{2}} \tag{4}$$

In this study, the root-mean-square values of the wavelet coefficients, W_{rms}, normalized by the maximum value of the wavelet coefficients, W_{max}, are plotted on the wavelet scale, a (m). The value has some peaks indicating periodic structures. The sequence scale, distance b (m) in this study, of the wavelet coefficients at the wavelet scale a (m), at which the coefficients show peak, was analyzed by Fourier transformation. Power spectrum of the wavelet coefficients in sequence scale determines the intensity of the periodic structure.

Results and Discussion

Figure 3 shows examples of interference patterns of 2-D grid turbulence. Vortices were generated at the comb in the flowing soap films and were convected in the observation area. The interference patterns of 2-D turbulence are used to visualize the thickness of water layer fluctuation, which is considered to be a passive scalar.[23,29,43] The characteristics of 2-D turbulence are an inverse energy cascade from small scale to large scale and an enstrophy cascade from large scale to small scale. The inverse energy cascade is visualized through the interference patterns of 2-D turbulence because the apparent size of the eddies in Figure 3a is larger than the injection scale. Through the addition of polymers, the eddies in the flows clearly become long in the streamwise direction and narrow in the normal direction. This feature is especially observed in the case of the addition of PEO, as shown in Figures 3b–d. This indicates that the polymer inhibits inverse energy transfers in the normal direction, therefore anisotropic deformations of vortices is occurred. For the case of the addition of HPC, deformations of vortices were also observed. However, the deformation was less anisotropic compared to PEO-added case. Such phenomena are precisely analyzed by FIFI, as described in the following.

An example of the power spectrum $<I^2(k_x, k_y)>$ of the interference pattern is shown in Figure 4. Figure 4a shows the 2-D representation of $<I^2(k_x, k_y)>$, where the darkness of the image indicates the intensity. The two arrows in the image indicate the direction corresponding to the streamwise and normal directions in the interference patterns. Here, k_x (m^{-1}) and k_y (m^{-1}) are the spatial frequencies, which contain information on the water layer fluctuations in the streamwise and normal directions, respectively. As an example, $<I^2(k_x, 0)>$ of the polymer free case is shown in Figure 4b, which shows the scaling behaviors. The power component of the power spectrum in Figure 4b is close to $-5/3$, which is in agreement with the passive scalar scaling

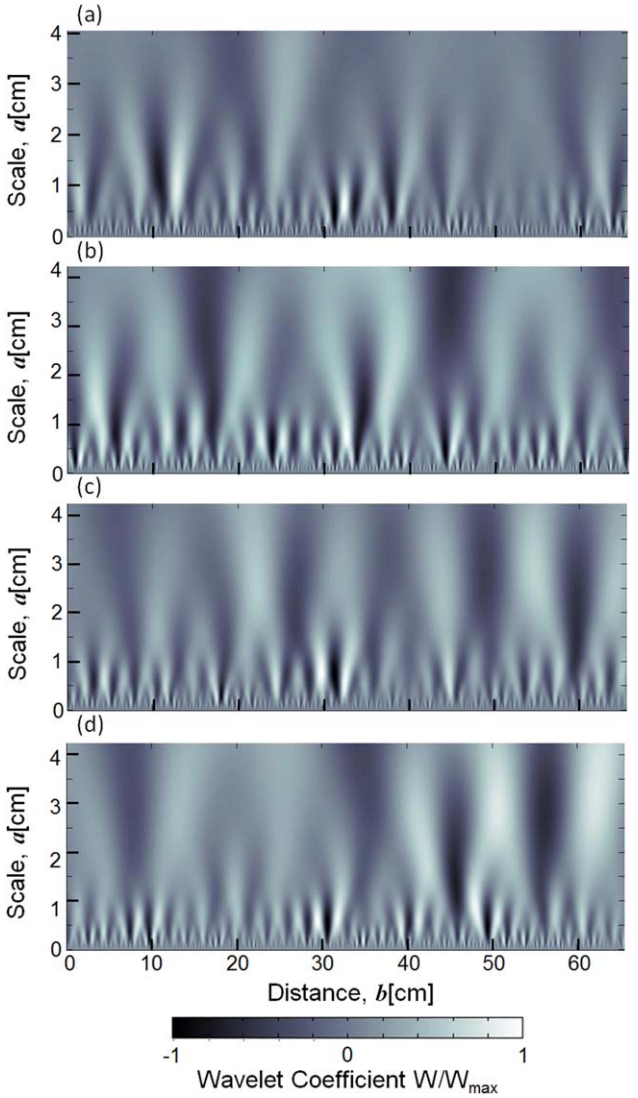

Figure 5. Wavelet coefficient contours for interference images.

(a) a SDBS 2 wt% solution, (b) a SDBS 2 wt% + PEO 0.25 × 10^{-3}-wt% solution, (c) a SDBS 2 wt% + PEO 0.5 × 10^{-3}-wt% solution, and (d) a SDBS 2 wt% + PEO 1.5 × 10^{-3}-wt% solution. [Color figure can be viewed in the online issue, which is available at wileyonlinelibrary.com.]

affected by inverse energy cascade and enstrophy cascade in 2-D turbulence. The variation of the power components is shown in Figures 4c, d. Figure 4c shows the variation when the PEO is added. In this case, the value was changed from $-5/3$ to -1 in both the streamwise and normal directions. At lower concentrations of PEO, the variation rate of the power component is low but increases rapidly from 0.5 to 0.75 × 10^{-3} wt%. Figure 4d shows the variation when the HPC is added. In this case, the value was changed gradually from $-5/3$ to -1 in the normal direction. However, in the streamwise direction, the variation of the scaling exponent was small. As aforementioned, the interference pattern is related to the thickness fluctuation. Thus, the power spectrum of the thickness fluctuation shows the power spectrum of passive scalars in 2-D flow. When passive scalars in 2-D flow are affected by both of inverse energy cascade and enstrophy cascade, the scaling

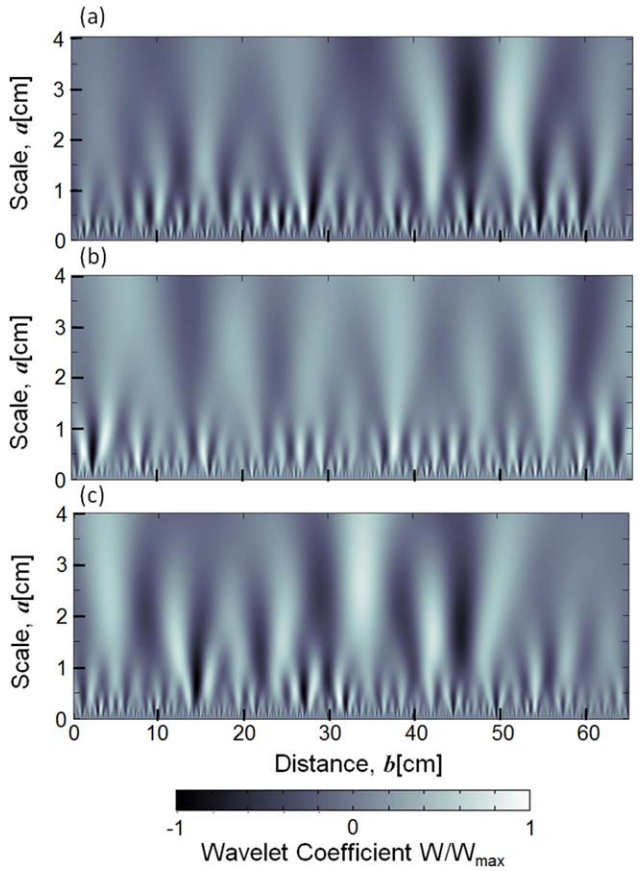

Figure 6. Wavelet coefficient contours for interference images.

(a) a SDBS 2 wt% + HPC 0.01 wt% solution, (b) SDBS 2 wt% + HPC 0.03 wt% solution, and a SDBS 2 wt% + HPC 0.05 wt% solution. [Color figure can be viewed in the online issue, which is available at wileyonlinelibrary.com.]

component of the power spectrum corresponds to −5/3. When passive scalars are affected by only enstrophy cascade, the scaling component of the power spectrum corresponds to −1. Therefore, such a variation of the scaling component from −5/3 to −1 directly related to the energy transfer in 2-D flow. Thus, from the basis of the variation of the scaling component, PEO is considered to prohibit the inverse energy cascade in both directions, whereas HPC prohibits the inverse energy cascade only in the normal direction. This difference is probably stemmed from the different energy-transfer mechanism in turbulence when polymers are added. In the normal direction, the orientation of the extended polymers may prohibit energy transfer in both the PEO-added and HPC-added cases. On the other hand, the extensional viscosity may prohibit energy transfer in the streamwise direction. This is because, when polymers were stretched and oriented parallel to the streamwise direction, polymers induce resistance in streamwise direction. Because the extensional viscosity of HPC is lower than that of PEO, HPC is less effective in prohibiting energy transfer in the streamwise direction. Such a variation of the energy transfer detected by the deformation of vortices in 2-D flows, which is related to the drag reduction effects. Indeed, in our previous study, we also analyzed the drag reduction effects of these PEO and HPC-added solution by measuring the friction coefficient in pipe flow.[31] The results from the pipe flow are consistent with the variation of scaling components.

Because the streamwise direction can be affected by extensional viscosity, wavelet transform is used for more detail analysis of the spatial fluctuation. Figures 5 and 6 show the wavelet coefficient contour for the pixel intensity $G(x)$ in the streamwise direction for the polymer-free solution (Figure 5a), the PEO-added solutions (Figures 5b–d), and the HPC-added solutions (Figure 6). In the figures, bright regions correspond to positive wavelet coefficients and dark regions correspond to negative wavelet coefficients. For the case of the polymer-free solution, it is hard to find periodic fluctuation in the wavelet scale, a (cm). Various scales of fluctuations appear irregularly in the wavelet contour. When the vortices are affected by increasing PEO concentration, relatively periodic fluctuation seems to be appeared in some wavelet scale, a (cm). In the case of HPC-added solution, relatively periodic fluctuation seems to appear at smaller wavelet scale. To determine how the periodic structures are changed by polymer concentration, the root mean square values of the wavelet coefficients, W_{rms}, normalized by the maximum value of the wavelet coefficients, W_{max}, are plotted on the wavelet scale (Figure 7). In the case of the polymer-free solution, only a broad peak is observed, which may be related to vortex size in 2-D

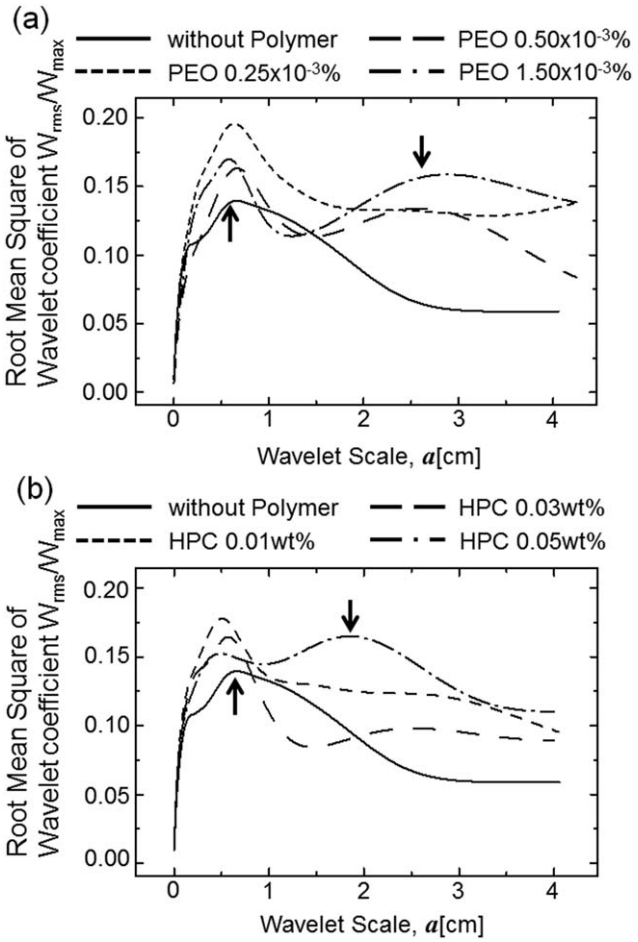

Figure 7. The root-mean-square value of the wavelet coefficient.

(a) the PEO-added solution. (b) the HPC-added solution. The arrows in the figure show the positions of the peaks at smaller and larger scales.

turbulence. This peak is enhanced by adding a low concentration of PEO at 0.25×10^{-3} wt%. The first peak, a (cm) is about 0.5 cm, decreases by increasing the concentration of PEO, and the other peak appears in larger wavelet scale, a (cm) is about 2.5 cm. At 2.0×10^{-3} wt%, the first peak in small wavelet scale is slightly shifted to a smaller scale, the second peak in large wavelet scale is shifted to a larger scale (Figure 7a). In the case of HPC, the first peak has similar tendency to the case of PEO, while the behavior of the second peaks are vague (Figure 7b). Figures 8 and 9 show the Fourier transform of the distance variation of the wavelet coefficients at the wavelet scale a (cm), where W_{rms} shows the maximum value at lower and larger scales. These results suggest that the original vortices in 2-D flow are going to disappear. The original fluctuations shifted to a higher and narrow frequency when the 2-D flow was affected by polymers. The other periodic structure appears in 2-D flow at lower and wider frequencies. Disappearance of vortices and appearance of lower frequency in the flow by adding polymers mean that the flow becomes anisotropic. This phenomenon is related to the drag reduction effects. Therefore, this wavelet analysis could detect the laminarization phenomena due to extensional viscosity by image analysis.

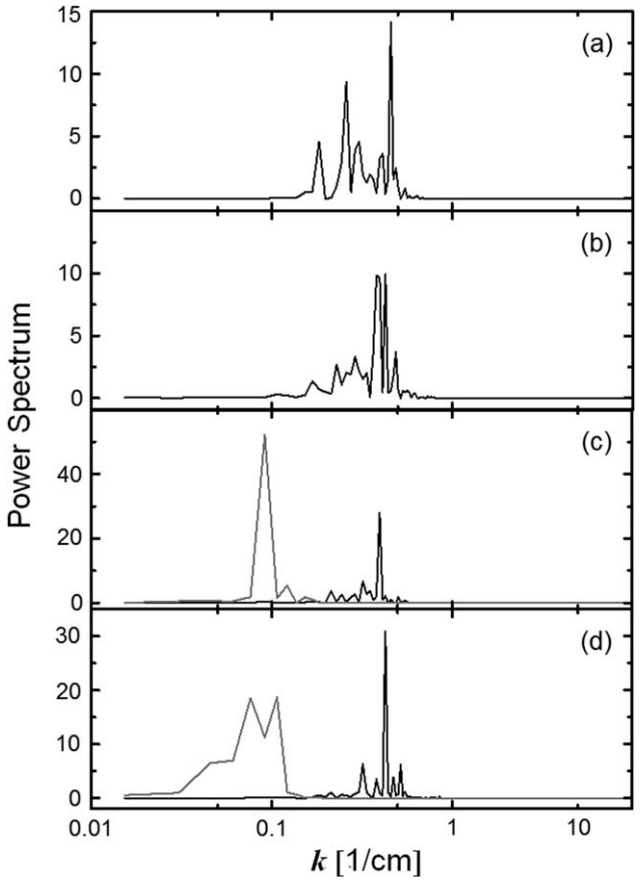

Figure 8. Power spectra of wavelet coefficients for SDBS- and PEO-added solutions.

(a)–(d) correspond to the solutions shown in Figure 5. When the peaks appear at smaller and larger scales, power spectrum was calculated at each position. Higher fluctuation is related to the smaller peak, and lower fluctuation is related to the larger peak.

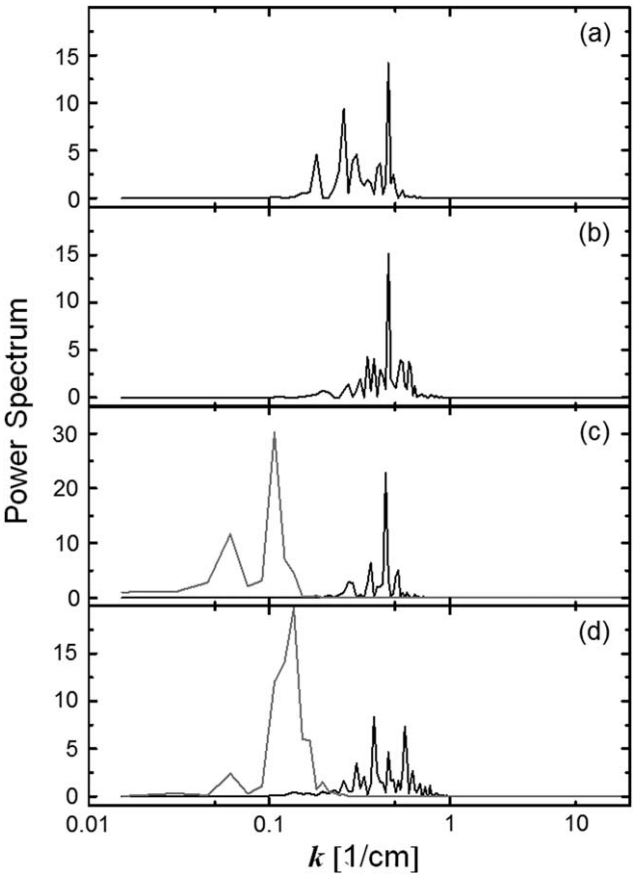

Figure 9. Power spectra of wavelet coefficients for SDBS- and HPC-added solutions.

(a)–(c) correspond to the solutions shown in Figure 6.

Conclusions

An experimental study has been performed to investigate how the extensional viscosity of polymers affects turbulent drag reduction. As flexible and rod-like rigid polymers, PEO and HPC, respectively, were added to the 2-D turbulent flow. Two-dimensional flow was realized by flowing soap films. Deformations of vortices affected by polymers in the 2-D flow were visualized through interference patterns of the soap films. Interference patterns were analyzed by Fourier transformation and wavelet analysis. Based on the results, the following conclusions were obtained:

1. Power spectra of interference images, which are related to the water layer fluctuations in turbulence, were obtained. The water layer fluctuations are passive scalar in 2-D flow. The scaling behavior of the power spectra provides information how passive scalars are affected by energy transfer in turbulence. In the normal direction, the power components were varied from $-5/3$ to -1 by adding polymers. The power components become -1 when the inverse energy cascade was ceased in the flow. Therefore, this variation indicates the prohibition of inverse energy transfers in 2-D turbulence by polymers. In the streamwise direction, the value was changed to -1 by adding PEO, whereas the value was slightly changed by adding HPC. These results suggest that the mechanism of drag reduction in turbulence differs depending on the direction. In the normal direction, the orientation of polymers prohibits

energy transfer, whereas the extensional viscosity prohibits energy transfer in the streamwise direction. The extensional viscosity of HPC is lower than that of PEO. Thus, HPC is less effective in the streamwise direction.

2. Wavelet coefficients were obtained by calculating the pixel intensity in the streamwise direction. When the root mean square values of the wavelet coefficients, W_{rms}, normalized by the maximum value of the wavelet coefficients, W_{max}, were plotted, two peaks were appeared. One is related to the original vortices, and the other is appeared when polymers affect flow. Variations of wavelet coefficient in distance scale at the peas were analyzed by Fourier transformation. By these analyses, it can be said that the original vortices are going to be disappeared, whereas the other low frequency structures appears. This indicates that the flow became anisotropic by adding polymers. This phenomenon is also related to the energy transfer in turbulence. This study can detect energy transfer related to drag reduction effects through vortices deformation in 2-D turbulent flows.

Acknowledgment

The present study was supported in part by a Grant-in-Aid for Young Scientists (B) (Project No.: 24760129) and a Grant-in-Aid for Scientific Research (B) (Project No.: 24360319) from the Japan Society for the Promotion of Science (JSPS).

Literature Cited

1. Toms BA. Some observations on the flow of linear polymer solutions through straight tubes at large Reynolds numbers. In: *Proceeding of the 1st International Congress on Rheology*, Scheveningen, Vol. 2, 1949;135–141.
2. Lumley J. Drag reduction by additives. *Ann Rev Fluid Mech.* 1969; 1:367–384.
3. Lumley J. Drag reduction in turbulent flow by polymer additives. *J Polym Sci.* 1973;7:263–270.
4. Virk PS. Drag reduction fundamentals. *AIChE J.* 1975;21:625–656.
5. Virk PS, Wagger DL. Aspects of mechanisms in type B drag reduction. In: *Structure of Turbulence and Drag Reduction*. IUTAM Symposium. Berlin, Springer, 1990; 201–213.
6. den Toonder JM, Hulsen MA, Kuiken GDC, Nieuwstadt FTM. Drag reduction by polymer additives in a turbulent pipe flow: numerical and laboratory experiments. *J Fluid Mech.* 1997;337:193–231.
7. Smith DE, Chu S. Response of flexible polymers to a sudden elongational flow. *Science*. 1998;281:1335–1340.
8. Sureshkumar R, Beris AN, Handler RA. Direct numerical simulation of the turbulent channel flow of a polymer solution. *Phys Fluids*. 1997;9:743–755.
9. Tamano S, Itoh M, Hoshizaki K, Yokota K. Direct numerical simulation of the drag-reducing turbulent boundary layer of viscoelastic fluid. *Phys Fluids.* 2007;19:075106-1–075106-17.
10. Hidema R, Furukawa H. Development of film interference flow imaging method (FIFI) studying polymer stretching effects on thin liquid layer. *e-J Surf Sci Nanotechnol.* 2012;10:335–340.
11. Reischman MM, Tiederman WG. Laser-Doppler anemometer measurements in drag reducing channel flows. *J Fluid Mech.* 1975;70:369–392.
12. van Doorn E, White CM, Sreenivasan KR. The decay of grid turbulence in polymer and surfactant solutions. *Phys Fluids*. 1999;11:2387–2393.
13. Jovanović J, Pashtrapanska M, Frohnapfel B, Durst F. On the mechanism responsible for turbulent drag reduction by dilute addition of high polymers: theory, experiments, simulations, and predictions. *J Fluids Eng*. 2006;128:118–130.
14. Procaccia I, L'vov VS, Benzi R. Theory of drag reduction by polymers in wall-bounded turbulence. *Rev Mod Phys.* 2008;80:225–247.
15. Cadot O, Bonn D, Douady S. Turbulent drag reduction by polymers. *J Phys Condens Matter*. 2005;17:S1195–S1202.
16. Housiadas KD, Beris AN. Polymer-induced drag reduction: effects of the variations in elasticity and inertia in turbulent viscoelastic channel flow. *Phys Fluids.* 2003;15:2369–2384.
17. Housiadas KD, Beris AN. An efficient fully implicit spectral scheme for DNS of turbulent viscoelastic channel flow. *J Nonnewton Fluid Mech.* 2004;122:243–262.
18. Housiadas KD, Beris AN. Characteristic scales and drag reduction evaluation in turbulent channel flow of nonconstant viscosity viscoelastic fluids. *Phys Fluids.* 2004;16:1581–1586.
19. Suzuki H, Higuchi Y, Watanabe H, Komoda Y, Ozawa S, Nishimura T, Takenaka N. Relaxation behavior of a drag-reducing cationic surfactant solution. *Nihon Reoroji Gakkaishi*. 2012;40:85–90.
20. Tamano S, Graham MD, Morinishi Y. Streamwise variation of turbulent dynamics in boundary layer flow of drag-reducing fluid. *J Fluids Mech.* 2011;686:352–377.
21. Wei T, Willmarth WW. Modifying turbulent structure with drag-reducing polymer additives in turbulent channel flow. *J Fluid Mech.* 1992;245:619–641.
22. Suzuki H, Nguyen H-P, Nakayama T, Usui H. Development characteristics of fluctuating velocity field of drag-reducing surfactant solution flow in a duct. *Rheol Acta*. 2005;44:457–464.
23. Kellay H, Goldburg WI. Two-dimensional turbulence: a review of some recent experiments. *Rep Prog Phys*. 2002;65:845–894.
24. Boffetta G, Ecke RE. Two-dimensional turbulence. *Ann Rev Fluid Mech.* 2012;44:427–451.
25. Couder Y. Two-dimensional grid turbulence in a thin liquid film. *J Phys (France) Lett.* 1984;45:353–360.
26. Couder Y. Experimental and numerical study of vortex couples in two-dimensional flows. *J Phys (France) Lett.* 1986;173:225–251.
27. Gharib M, Derango P. A liquid film (soap film) tunnel to study two-dimensional laminar and turbulent shear flows. *Physica D*. 1989;37: 406–416.
28. Rutgers MA, Wu XL, Daniel WB. Conducting fluid dynamics experiments with vertically falling soap films. *Rev Sci Instrum.* 2001;72:3025–3037.
29. Amarouchene Y, Kellay H. Polymers in 2D turbulence: suppression of large scale fluctuations. *Phys Rev Lett.* 2002;89:104502–1–104502-4.
30. Batchelor GK. Computation of the Energy Spectrum in homogeneous two-dimensional turbulence. *Phys Fluids. Supplement II*. 1969; 12:II 233–II 239.
31. Hidema R, Yatabe Z, Shoji M, Hashimoto C, Pansu R, Sagarzasu G, Ushiki H. Image analysis of thickness in flowing soap films. I: effects of polymer. *Exp Fluids*. 2010;49:725–732.
32. Hidema R, Ushiki H, Furukawa H. Polymer effects on turbulence in flowing soap films studied with film interference flow imaging method. *J Solid Mech Mater Eng*. 2011;5:838–848.
33. Hidema R, Suzuki H, Hisamatsu S, Komoda Y, Furukawa H. Effects of the extensional rate on two-dimensional turbulence of semi-dilute polymer solution flows. *Rheol Acta*. 2013;52:949–961.
34. Hetsroni G, Zakin JL, Mosyak A. Low-speed streaks in drag-reduced turbulent flow. *Phys Fluids.* 1997;9:2397–2404.
35. Li C-F, Sureshkumar R, Khomami B. Influence of rheological parameters on polymer induced turbulent drag reduction. *J Nonnewton Fluid Mech.* 2006;140:23–40.
36. Wilczek M, Kadoch B, Schneider K, Friedrich R, Farge M. Conditional vorticity budget of coherent and incoherent flow contributions in fully developed homogeneous isotropic turbulence. *Phys Fluids.* 2012;24:035108–035122.
37. Farge M. Wavelet transforms and their applications to turbulence. *Ann Rev Fluid Mech.* 1992;24:395–457.
38. Do-Khac M, Basdevant C, Perrier V, Dang-Tran K. Wavelet analysis of 2D turbulent fields. *Physica D*. 1994;76:252–277.
39. Farge M, Schneider K, Kevlahan N. Non-Gaussianity and coherent vortex simulation for two-dimensional turbulence using an adaptive orthogonal wavelet basis. *Phys Fluids*. 1999;11:2187–2201.
40. Rinoshika A, Omori H. Orthogonal wavelet analysis of turbulent wakes behind various bluff bodies. *Exp Therm Fluid Sci*. 2011;35: 835–845.
41. Tirtaatmadja V, McKinley GH, Cooper-White JJ. Drop formation and breakup of low viscosity elastic fluids: effects of molecular weight and concentration. *Phys Fluids*. 2006;18:043101-1–043101-18.
42. Belmonte A, Martin B, Goldburg WI. Experimental study of Taylor's hypothesis in a turbulent soap film. *Phys Fluids.* 2000;12:1231–1238.
43. Rivera M, Vorobieff P, Ecke RE. Turbulence in flowing soap films: velocity, vorticity, and thickness fields. *Phys Rev Lett*. 1998;81: 1417–1420.

Manuscript received Jun. 4, 2013, and revision received Nov. 5, 2013.